



VTT Technical Research Centre of Finland

High-performance silicon-based nano-thermoelectric bolometers for uncooled infrared sensing

Varpula, Aapo; Murros, Anton; Sovanto, Kuura; Rantala, Arto; Martins, David Gomes; Tappura, Kirsi; Tiira, Jonna; Prunnila, Mika

Published in:
Electro-Optical and Infrared Systems

DOI:
[10.1117/12.2675913](https://doi.org/10.1117/12.2675913)

Published: 01/01/2023

Document Version
Peer reviewed version

[Link to publication](#)

Please cite the original version:

Varpula, A., Murros, A., Sovanto, K., Rantala, A., Martins, D. G., Tappura, K., Tiira, J., & Prunnila, M. (2023). High-performance silicon-based nano-thermoelectric bolometers for uncooled infrared sensing. In D. L. Hickman, H. Bursing, G. W. Kamerman, & O. Steinvall (Eds.), *Electro-Optical and Infrared Systems: Technology and Applications XX* Article 1273702 International Society for Optics and Photonics SPIE.
<https://doi.org/10.1117/12.2675913>

VTT
<https://www.vttresearch.com>

VTT Technical Research Centre of Finland Ltd
P.O. box 1000
FI-02044 VTT
Finland

By using VTT Research Information Portal you are bound by the following Terms & Conditions.

I have read and I understand the following statement:

This document is protected by copyright and other intellectual property rights, and duplication or sale of all or part of any of this document is not permitted, except duplication for research use or educational purposes in electronic or print form. You must obtain permission for any other use. Electronic or print copies may not be offered for sale.

High-performance silicon-based nano-thermoelectric bolometers for uncooled infrared sensing

Aapo Varpula^{*a}, Anton Murros^a, Kuura Sovanto^a, Arto Rantala^a, David Gomes Martins^a,
Kirsi Tappura^a, Jonna Tiira^a, Mika Prunnila^a

^aVTT Technical Research Centre of Finland Ltd, Tietotie 3, FI-02150 Espoo, Finland

ABSTRACT

Infrared (IR) sensors and photodetector arrays are employed in various imaging applications (such as night vision), remote temperature measurement, and chemical analysis. These applications are in space and environmental sensing, transport, health and medicine, safety, security, defense, industry, agriculture, etc. Optical chemical analysis employs IR absorption spectroscopy which enables the identification and quantification of gases, liquids, and materials based on their unique absorption spectra which are feature-rich in the IR region.

State-of-the-art (SoA) quantum photodetectors utilize either photoconductivity or the photovoltaic effect. Commercial quantum photodetectors are widely available in the spectral range from UV to short-wave infrared (SWIR), but in mid-wave IR (MWIR) and long-wave IR (LWIR), they require exotic materials and cooling to maintain high sensitivity. Thermal detectors (bolometers) are a competing technology that can reach high sensitivities in IR without the need for cooling and can be manufactured using widely available semiconductor technologies. SoA bolometers include resistive bolometers, diode- or transistor-based bolometers, and thermoelectric bolometers. By utilizing nanomaterials and integrated design, we have minimized the thermal mass and demonstrated fast and sensitive nano-thermoelectric IR bolometers with high thermoelectric efficiency.

We review the application and development of the silicon-based nano-thermoelectric infrared bolometers: modelling, design, fabrication, and electro-optical characteristics. The enabling materials, silicon nanomembranes, are also discussed, and the first devices used to test the potential of these nanomembranes, the electro-thermal devices, are reviewed and new experimental results are presented.

Keywords: Infrared detector, nano-thermoelectrics, mid-wavelength infrared, long-wavelength infrared, thermoelectric bolometer, nanomembrane, silicon

1. INTRODUCTION

Infrared (IR) sensors operating in the short- (SWIR), mid- (MWIR) and long-wave IR (LWIR) regions have various applications ranging from thermal imaging for night vision to remote thermometry and chemical analysis using infrared spectroscopy¹⁻³. These applications find use in sectors such as space and environment sensing, transport, health and medicine, safety, security, defense, industry, and agriculture. Targeting the longer wavelengths – MWIR and LWIR – offers possibilities for gathering independent spectral information with passive operation by utilizing the background thermal emission of objects whose IR emission is strongest in this range¹. IR detection in this range can be utilized for example in optical chemical analysis employing IR absorption spectroscopy to identify and quantify gases, liquids, and materials based on their unique IR absorption spectra^{1,2}.

The most commonly commercially available IR sensors are quantum detectors based on electron-hole pair generation, and thermal detectors (bolometers) based on radiation-induced heating of an absorber. Quantum detectors typically provide higher performance than bolometers in terms of speed and sensitivity. However, quantum detectors require cooling down from room temperature to cryogenic temperatures to reach their maximum performance, particularly in the LWIR range where photon energies are small⁴. Quantum detectors in the LWIR range also require expensive and toxic materials, such as HgCdTe and InAsSb⁴. On the other hand, state-of-the-art bolometers can reach relatively high sensitivities without cooling and can be manufactured using widely available CMOS-compatible technologies.

*aapo.varpula@vtt.fi; phone 358 40 357-1370; vttresearch.com

Furthermore, by leveraging nano-thermoelectrics – wherein the material properties of the thermoelectric elements are improved by dimensional scaling to the sub-100nm regime – bolometer performance can be improved, and the signal transduction noise can be significantly reduced, leading to a low noise transduction method for thermal sensors^{5,6} and bolometers^{4,7}. These benefits in conjunction with smart IR detector design allow thermoelectric bolometers to be a competitive technology to SoA quantum detectors, narrowing the gap between cooled and uncooled IR photodetector technologies⁴.

It has been demonstrated that by reducing the thickness of silicon in two-dimensional systems, i.e. thin films, the thermal conductivity can be reduced by almost two orders of magnitude^{8,9}. Experiments have consistently shown that a reduction in the silicon membrane thickness results in a proportional reduction in thermal conductivity^{8,10–13}, with an observed experimental minimum thermal conductivity of 9 W/mK measured in a 9-nm free-standing silicon membrane⁸. The reduction in thermal conductivity can be attributed to the spatial confinement of phonon modes in thin films^{14–16} and increased phonon scattering at boundaries resulting in shortened phonon mean free path^{17–19}. To maximize the thermoelectric figure of merit ZT , and therefore achieve high thermoelectric detector performance, the reduction in thermal conductivity must be balanced without compromising electrical conductivity. This challenges some nanostructuring methods, such as nanomeshes²⁰ and nanoholes²¹, as a method to achieve large reductions in thermal conductivity, since the presence of pores and grain boundaries can reduce charge transport as well⁹. On the other hand, thickness reduction may enhance Seebeck coefficient and electron mobility due to quantum confinement^{22–26}.

We have demonstrated nano-thermoelectric IR bolometers^{4,7} based on ultra-thin silicon membranes. They utilize silicon nanomembranes as phonon-engineered thermoelectric elements with enhanced ZT and metal nanomembranes and low thermal mass absorbers. The principle of operation of the IR bolometer is illustrated in Figure 1. Incident IR radiation is converted into a temperature change by the absorber element, which is thermally isolated from the ambient and substrate by suspension with support beams. Typically, the detector is sealed in a low thermal conductivity atmosphere or vacuum. The support beams are thermoelectric n- and p-type doped Si nanomembranes that act as thermocouple elements to convert the induced temperature gradient between the absorber and ambient (or substrate) into an electrical signal via the Seebeck effect. This mode of operation enables low power operation, as the bolometer does not require any external power for signal generation.

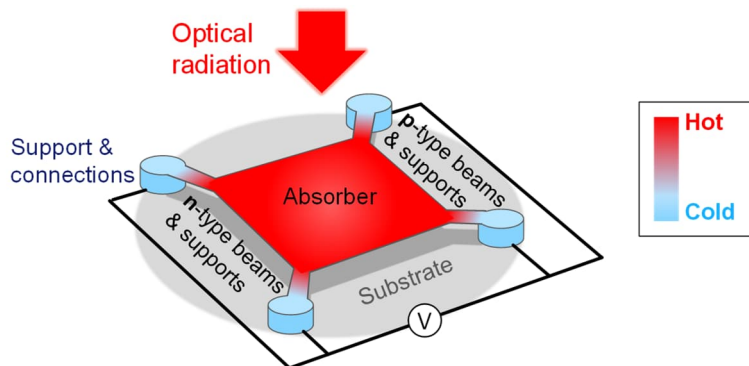


Figure 1. Schematic picture of a thermoelectric bolometer supported by 4 beams⁷. 2-beam bolometers with the same principle are also common. During the operation, the absorber absorbs the incident optical radiation and heats up. The formed temperature gradient is converted into electric voltage using p- and n-type thermoelectric materials (i.e., legs) placed in/on the supporting beams, or they can act simultaneously as supports themselves⁴.

Thermoelectric transduction via the Seebeck effect has in principle low noise, with the main noise sources being Johnson-Nyquist and thermal fluctuation noise^{5,27,28}. By scaling down the size of the thermocouple beams the phonon thermal conductance can be reduced, potentially allowing the devices to reach thermal fluctuation noise limited performance⁶. The thermal mass of the detectors is minimized by the absence of separate micromechanical supporting layers and by the integrated metal nanomembrane absorber. Further thermal mass reduction and thermal conductivity reduction is achieved by reducing the cross-sectional dimensions of the device. The reduced thermal mass enables high-

speed operation, which can also be exploited as increased sensitivity by altering the design of the bolometer in terms of beam dimensions, detector area, absorber fill factor, and film thicknesses.

In this article we review the development of the silicon-based nano-thermoelectric infrared bolometers. In section 2, the modelling of thermoelectric bolometers^{4,7,29,30} is discussed. In section 3, we discuss the key enabling materials, silicon nanomembranes, and their fabrication processes for realizing the dimensionality reduction³⁹. The availability of nanomembranes leads to the realization of nano-thermoelectric electro-thermal devices^{5,6}, which are discussed with new experimental results in section 4. Finally, the experimental IR bolometers^{4,7} are discussed in section 5 and their estimated performance potential in section 6. We are also working on the readout integrated circuits, which are discussed in Ref. [7].

2. MODELING OF THERMOELECTRIC BOLOMETERS

2.1 Device model of thermoelectric bolometers

Thermoelectric bolometers are described by a combination of thermal resistor-capacitor (RC) and thermoelectric models^{4,29,30}. The speed of a bolometer is described by thermal time constant

$$\tau = \frac{C_{th}}{G_{th}}, \quad (1)$$

where C_{th} is the thermal capacitance, i.e. the heat capacity, of the bolometer, and G_{th} is the thermal conductance of the bolometer (i.e. the thermal conductance between the absorber and the substrate and surroundings). The corresponding thermal cutoff angular frequency is $\omega_c = 1/\tau$. At frequencies well below ω_c , the dependence of the output voltage of a thermoelectric bolometer on the incident optical power P is characterized by the (voltage) responsivity⁴

$$R_V = \left. \frac{dV}{dP} \right|_{\omega \ll \omega_c} = \frac{S\eta}{G_{th}}, \quad (2)$$

where the total Seebeck coefficient of the thermoelectric transducer of the bolometer is given by $S = S_p - S_n$, where S_p and S_n are the Seebeck coefficients of the p- and n-type thermoelectric elements, and η is the optical efficiency of the absorber.

The sensitivity of a detector is determined by the combination of the responsivity and noise. In thermoelectric bolometers there are the two dominant noise sources; the Johnson-Nyquist noise and the thermal fluctuation noise. The optical noise-equivalent power (NEP) corresponding to the Johnson-Nyquist noise is given by

$$NEP_{JN} = \frac{\sqrt{4k_B T R}}{R_V}, \quad (3)$$

where k_B is Boltzmann's constant, T the absolute temperature, and R the (total) resistance of the bolometer. The optical NEP corresponding to the thermal fluctuation noise is given by $NEP_{th} = \sqrt{4k_B T^2 G_{th}}/\eta$. These noise sources can be combined into total NEP as^{4,29,5}

$$NEP = \sqrt{NEP_{th}^2 + NEP_{JN}^2} = NEP_{th} \sqrt{1 + \frac{1}{\widetilde{ZT}}}, \quad (4)$$

where the effective thermoelectric figure of merit of the bolometer is given by

$$\widetilde{ZT} = \frac{S^2 T}{G_{th} R}. \quad (5)$$

The specific detectivity D^* allows for comparison of different detector technologies and detectors with different active areas. It is given by

$$D^* = \frac{\sqrt{A_{abs}}}{NEP}, \quad (6)$$

where A_{abs} is the area of the absorber.

2.2 Model of quarter-wave resistive absorber

A quarter-wave resistive absorber illustrated in Fig. 2 is a radiofrequency and optical absorber design which allows effective absorption in bolometers^{4,7,29}. It is also known as the Salisbury screen^{29,31} or an antiresonant interference structure³². A quarter-wave resistive absorber consists of a conducting film and a reflector. The conducting film is placed near the reflector so that an optical cavity is formed. The optical absorption of the structure is maximized when the real or effective sheet resistance of the absorber is matched to the vacuum impedance.

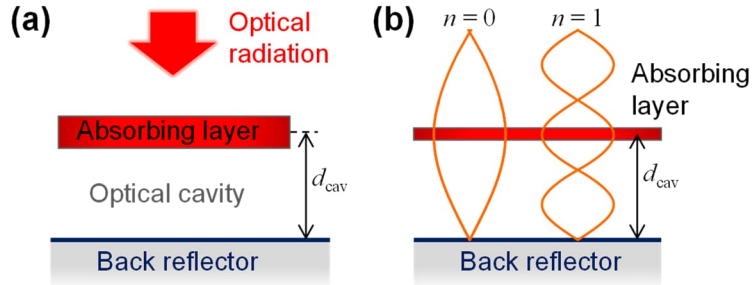


Figure 2. (a) Schematic cross-section of the quarter-wave absorber²⁹. The absorbing layer placed above a back reflector. Optical cavity with the depth of d_{cav} is formed between the back reflector and the absorbing layer. (b) Illustration of optical waves in the absorber in the cases corresponding to two absorption peaks with the longest matching wavelengths, i.e. orders $n = 0$ and $n = 1$ ²⁹. The optical absorption is strongest when an antinode of the optical wave is on the absorbing layer.

The optical properties of the quarter-wave resistive absorber structure can be modelled with full-wave electromagnetic simulations⁴, transfer-matrix model²⁹, or analytical optical model²⁹ derived from a radio-frequency model of the Salisbury screen³³. The first model is the most general one suitable for complex absorber geometries, but it is computationally heavy as it requires use of the finite-element method (FEM). The transfer matrix model^{34,35} describes uniform layers of optical media, and this reduces the computational load considerably. This approach is often suitable for bolometers as their absorbers can be modelled using effective materials. We have shown that the fully analytical optical model matches with the transfer matrix model in idealized cases and agrees reasonably well in realistic cases²⁹. The analytical model enables very rapid calculations.

In the analytical model, the absorption spectrum of an ideal quarter-wave resistive absorber consists of periodic absorption peaks at the wavelengths²⁹

$$\lambda_{peak} = \frac{4d_{cav}}{1 + 2n}, \quad (7)$$

where d_{cav} is the depth of the cavity and the order $n = 0, 1, 2, 3, \dots$. The relative bandwidth of the peak with the lowest matching wavelength ($n = 0$) is rather broad: 280 % relative full-width-at-half-maximum (FWHM) bandwidth²⁹. The cavity depth d_{cav} defines the spectral range of the structure. At the wavelengths of eq. (7), the absorptance of an ideal quarter-wave absorber is given by^{7,29}

$$A = \frac{4 \frac{Z_{vac}}{R_{sh}}}{\frac{Z_{vac}}{R_{sh}} \left(\frac{Z_{vac}}{R_{sh}} + 2 \right) + 1}, \quad (8)$$

where the vacuum impedance, or the impedance of free space, is $Z_{vac} \approx 376.73 \Omega$ and R_{sh} is the (effective) sheet resistance of the absorber. Eq. (8) is plotted in Fig. 3, showing that rather high absorption can be achieved with a wide range of sheet resistance R_{sh} values (for example for $A > 50\%$, R_{sh} can range between 65 and 2196 Ω ²⁹).

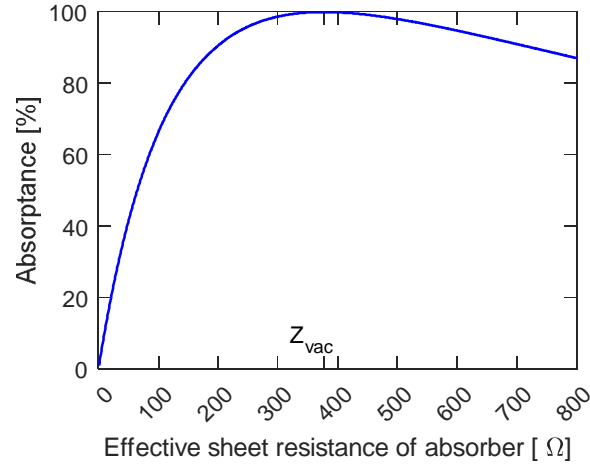


Figure 3. Dependence of absorptance A of the ideal quarter-wave resistive absorber on the effective sheet resistance of the absorber R_{sh} and vacuum impedance $Z_{vac} \approx 376.73 \Omega$, when the wavelength of the optical signal is at the maximum of an absorber peak. Calculated using eq. (9).

The full dependence of the absorptance A on wavelength λ is given by

$$A = \frac{4 \frac{Z_{vac}}{R_{sh}} \left[\sin \left(\frac{2\pi d_{cav}}{\lambda} \right) \right]^2}{\frac{Z_{vac}}{R_{sh}} \left(\frac{Z_{vac}}{R_{sh}} + 2 \right) \left[\sin \left(\frac{2\pi d_{cav}}{\lambda} \right) \right]^2 + 1}. \quad (9)$$

Figure 4 shows a comparison between the transfer-matrix and analytical model in the cases of pure conductor and metallic VO₂ as a quarter-wave resistive LWIR absorber. The transfer matrix and the analytical models agree very well in the case of the pure conductor. In the VO₂ case, the peaks are slightly distorted and decay towards the smaller wavelengths. The decay is caused by the Drude-behavior of the complex permittivity and the imaginary part of the electric conductivity, which are present in real materials²⁹. Despite these deviations, the analytical model is a powerful tool for rapid bolometer design drafting and description of the absorber behavior.

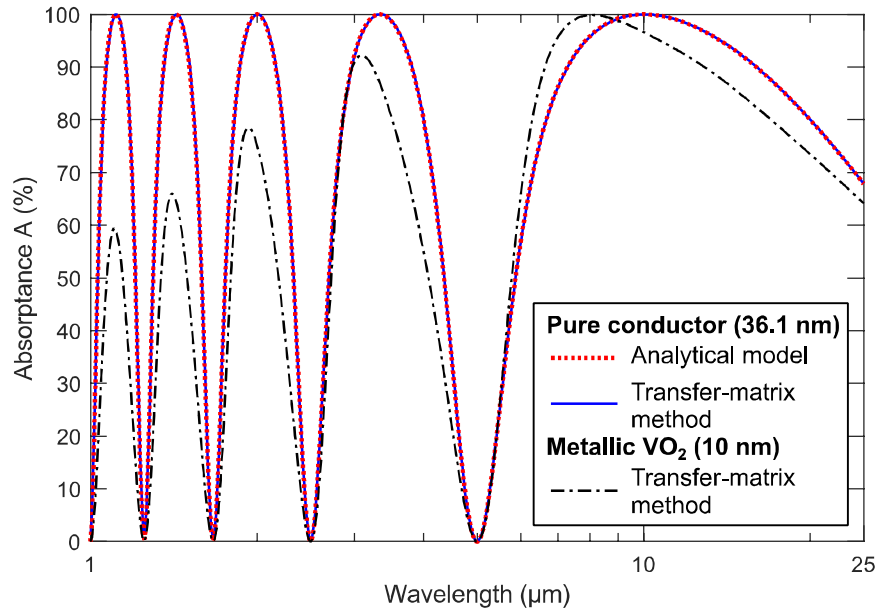


Figure 4. Comparison of absorption spectra of a quarter-wave resistive absorber calculated using the analytical model [eq. (9)] and the transfer-matrix method²⁹. The depth of the optical cavity is $d_{cav} = 2500$ nm. Here the exemplary absorbing layer is metallic VO₂, which is modeled either as a pure conductor with the experimental DC electric conductivity or using experimental n and k data²⁹.

3. NANO-THERMOELECTRIC SILICON MEMBRANES

Silicon is an attractive detector material due to its common use in the semiconductor industry, and its cost-efficient, non-toxic, and generally abundant nature. However, due to its high thermal conductivity of 148 W/mK in the bulk³⁶, silicon has a low thermoelectric figure of merit, ZT , at room temperature $ZT_{300K} \approx 0.01$ ^{8,9}. By shaping silicon into nano-scale membranes^{8,37} or wires³⁸, the thermal conductance of silicon is significantly reduced – whilst preserving Seebeck coefficient and electrical conductivity virtually unaltered – resulting in a significantly improved ZT ^{5,4}. By leveraging nano-thermoelectrics in this manner, Si-based nanostructures form an extremely promising transducer materials platform for thermoelectric detectors.

Previously, we reported on the fabrication and characterization of large-area ultra-thin flat suspended single-crystalline (SC) Si membranes with controlled strain with membrane thicknesses down to 6 nm³⁹. For more details, refer to Ref. [39]. The produced devices were thermally studied by Chávez-Ángel and co-workers⁸ to produce the results shown in Figure 5. The fabrication process³⁹ involves thinning down a SOI layer by thermal oxidation and subsequent oxide removal to produce a Si film of the desired thickness. A Si₃N₄ film under tensile stress is deposited by low-pressure chemical vapor deposition (LPCVD) and patterned to form a stress-compensating frame that allows for compensation of compressive stress and strain tuning of the Si membrane. This stress-compensating frame is also utilized in our IR bolometers, discussed further in sections 4 and 5. Finally, the Si membranes were released by backside deep etching through the wafer.

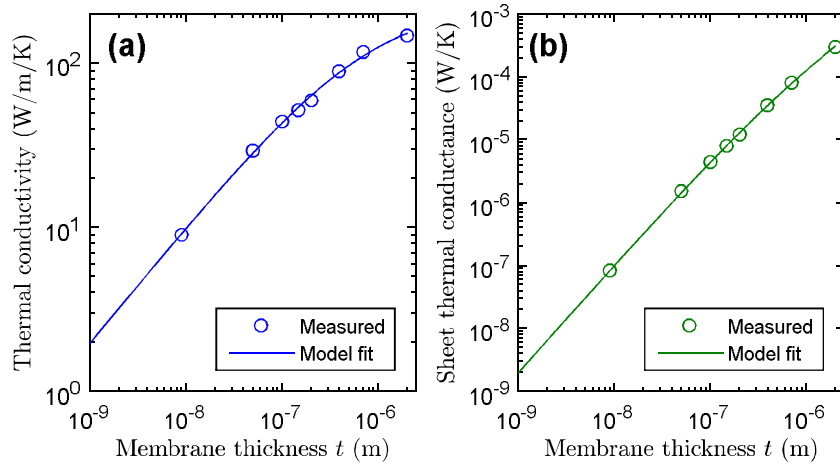


Figure 5. Experimental data⁸ and fitted phenomenological model³⁰, $\kappa = \alpha/(1 + \beta t^\gamma)$, of (a) thermal conductivity κ and (b) sheet thermal conductance $G_{\text{th}} = \kappa t$ of ultra-thin single-crystalline silicon membranes as functions of membrane thickness t . The values of the model fitting parameters are $\alpha = 228.4$ W/m/K, $\beta = 116.0$ /nm, and $\gamma = 0.7149$.

The thermal conductivity and conductance of ultra-thin single-crystalline silicon membranes as a function of membrane thickness are shown in Figure 5. For modeling purposes, a phenomenological model has been fitted to the measured data. The reduction in silicon membrane thickness results in almost two-orders of magnitude decrease in thermal conductivity, with an observed experimental minimum thermal conductivity of 9 W/(mK) in a 9-nm free-standing silicon membrane⁸. The reduction of thermal conductivity is caused by the spatial confinement of phonon modes in thin films^{14–16} and increased phonon scattering at boundaries resulting in shortened phonon mean free path^{17–19}. Reducing the thickness of the thermoelectric membrane is an effective method to improve ZT and therefore achieve high thermoelectric detector performance without significantly sacrificing electrical conductivity. Thickness scaling is thus an attractive solution to enable room temperature high-sensitivity and cost-effective IR detection.

Nano-thermoelectric Si can be realized by doping the nanomembranes into n- and p-type Si^{5–4}. In addition to SC-Si, poly-crystalline Si nanomembranes can also be realized⁶. While higher charge-carrier mobilities allow lower resistivities to be obtained with SC-Si than with poly-Si, poly-Si affords simpler and more cost-efficient device fabrication. The characteristics of the nano-thermoelectric SC- and poly-Si are shown in Table 1. These were obtained from electro-thermal devices and IR bolometers which are described in sections 4 and 5. The Seebeck coefficients in Table 1 were measured with electro-thermal devices (see section 4) by employing the heater resistors as thermometers and thermocouples as Peltier coolers and heaters^{5,6}.

Table 1. Microstructure and thermoelectric properties of nano-thermoelectric silicon membranes. The total Seebeck coefficients were measured using electro-thermal devices^{5,6}.

Crystallinity	Membrane thickness	N-type resistivity	P-type resistivity	Total Seebeck coefficient S	Ref.
Single	40 nm	1.9 mΩcm	1.8 mΩcm	0.39 mV/K	[5]
Poly	100 nm	11 mΩcm	9.7 mΩcm	0.59 mV/K	[6]
Poly	80 nm	5.3 mΩcm	3.4 mΩcm	-	[4]
Poly	70 nm	4.7 mΩcm	3.0 mΩcm	-	[4]

4. ELECTRO-THERMAL DEVICES

We have investigated the potential of nano-thermoelectric silicon membranes in sensor and detector devices by fabricating electro-thermal devices out of them. These electro-thermal devices have a resistor for heating and a thermocouple for measuring thermal output voltage^{5,6}. They are excellent vehicles for investigating the performance prospects of these materials. These devices can also be used as direct thermal detectors, for example in scientific experiments with scanning thermal microscopy (SThM)^{40,41}.

The scanning-electron microscopy (SEM) and optical microscopy images of the fabricated electro-thermal devices are shown in Figure 6. These devices utilize a silicon nitride (Si_xN_y) stress-compensation frame to control the strain of the nanomembrane^{5,6,39}. In the devices the silicon nanomembranes are patterned into beams supporting a membrane section in the middle. In the middle membrane, there are meandering heater resistors made by doping this part of the membrane with boron (p+). The beams are also either n+ or p+ doped to provide electrical contact to the heater and to form the thermocouple together with aluminum contact metal.

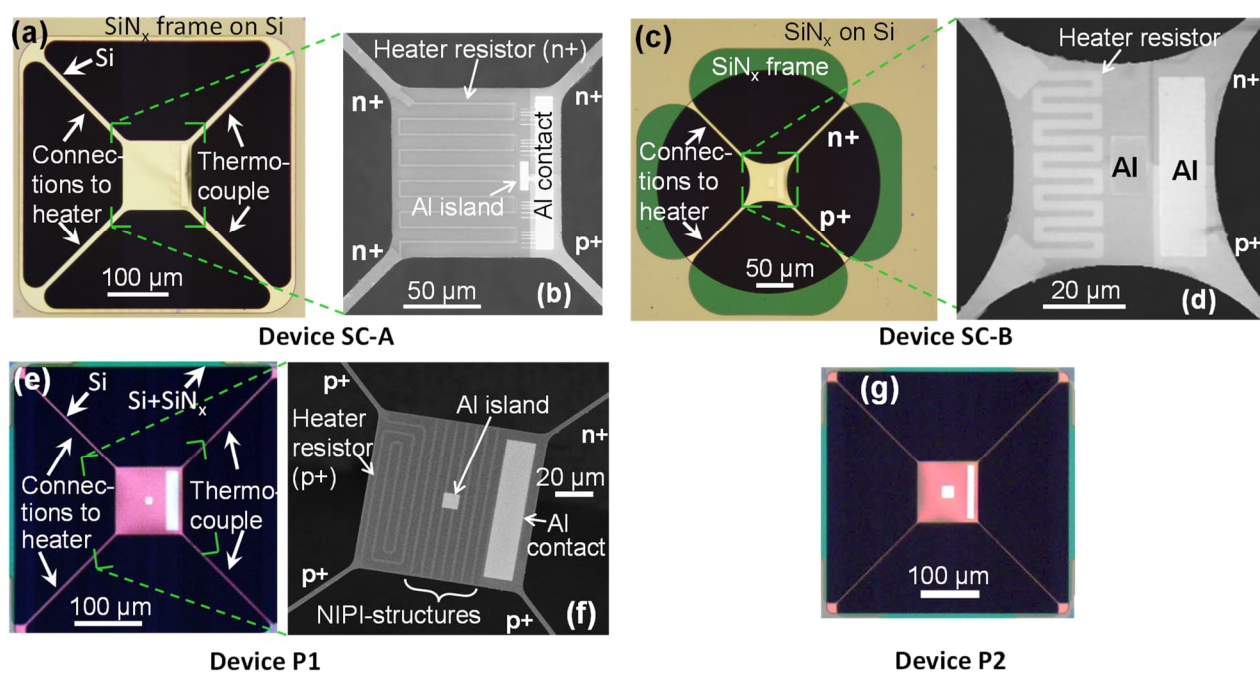


Figure 6. Optical (a, c, e, g) and scanning-electron (b, d, f) micrographs of devices SC-A⁵ (a, b), SC-B⁵ (c, d), P1⁶ (e, f), and P2 (g). These electro-thermal devices have electric heater resistors for characterization and experimentation, and a thermocouple for electric temperature readout. The pair of the silicon beams on the left side of the devices provides the electrical connection for the meandered doped silicon heater resistor patterned in the silicon membrane. The 30-nm Al film forms an electrical contact between the ends of the n+ and p+ silicon beams acting as thermocouple. The devices have Al islands for scanning probing experiments. Device P1 has additional alternating n+ doped, undoped, and p+ doped regions (NIPI) between the heater meanders and the heater and the thermocouple to ensure that the heater is well electrically insulated from the rest of the device⁶.

The electro-thermal devices were fabricated on 150-mm silicon wafers using the fabrication processes described in Refs. [5, 6]. In the case of single-crystalline (SC) Si devices, silicon-on-insulator (SOI) wafers were used. The targeted single-crystalline nanomembrane thickness was reached by thinning down the SOI layer by thermal oxidation and oxide stripping. In case of polycrystalline Si devices, standard silicon wafers were first oxidized to form a buried silicon oxide, and then a layer of 100 nm polysilicon was added by LPCVD on them. Next, both Si layers were doped selectively with boron and phosphorus by ion implantation and patterned by plasma etching. Then, a 280-nm-thick stress-compensation Si_xN_y layer was deposited by LPCVD. Next, a 30-nm-thick layer of Al (contact metal) was sputtered and patterned by wet

etching. Finally, the devices were released by deep-reactive etching through the silicon wafer from the back side and HF vapor etching of the buried oxide layer.

The measured characteristics of the electro-thermal devices are summarized in Table 2. The thermal time constants fall into the range 2.5–30 ms and are governed by the thickness of the Si nanomembranes, size of the middle membrane, and the dimensions of the supporting beams. Due to this, the thinner single-crystalline devices are faster. Noise measurements⁵ have confirmed the theoretical prediction that the noise in these devices is fully described by the Johnson-Nyquist noise originating from the electrical resistance of the thermocouple. The NEPs in Table 2 were calculated using eq. (3) with electric responsivity, which is eq. (2) in the case $\eta = 1$. The poly-Si devices have larger responsivities mainly due to the larger Seebeck coefficient of the poly-Si (see Table 1), but the higher resistivity of the poly-Si (see Table 1) increases the thermocouple resistances leading to higher noise, which compromises NEP. The device beam dimensions have also an effect, which can be clearly seen between devices SC-A and SC-B, and P1 and P2. Overall, these electro-thermal devices are suitable for rapid detection of small thermal signals.

Table 2. Characteristics of electro-thermal devices^{5,6}.

Device	Material	Middle membrane size [μm^2]	Thermal time constant τ [ms]	Electrical responsivity [V/W]	Thermocouple resistance [k Ω]	Electrical NEP [pW/Hz ^{1/2}]
SC-A ⁵	40 nm SC-Si	110 x 110	9.4 ms	1180	27	18
SC-B ⁵	40 nm SC-Si	50 x 50	2.5 ms	1960	39	13
P1 ⁶	100 nm poly-Si	100 x 100	13 ms	3090	215	19
P2	100 nm poly-Si	100 x 100	30 ms	6750	797	17

5. EXPERIMENTAL NANO-THERMOELECTRIC INFRARED BOLOMETERS

We have demonstrated nano-thermoelectric bolometers operating in the LWIR regime, targeted to maximize detector output for room-temperature thermal radiation with a wavelength maximum of approximately 10 μm ^{4,7}. Our bolometers have been fabricated with nano-thermoelectric silicon membranes that operate as both a signal transducer – converting the thermal signal into electrical output – and as mechanical supports for the integrated metal absorber. By utilizing the properties of nano-thermoelectric membranes and smart device design, the thermal mass and conductivity of the detectors can be tuned and optimized to target different application ranges, preferring high sensitivity or fast operation speed⁴.

Scanning electron micrographs of the fabricated bolometers with cross-sectional device schematics are shown in Figure 7. The devices consist of an optical absorber supported by integrated n- and p-type ultra-thin silicon membranes, which act as thermocouples transducing incoming IR radiation into electrical signal. The metal optical absorber electrically connects the thermocouple pair and also acts as an infrared absorber, converting incoming IR radiation into a temperature change that is utilized by the thermocouples. Additionally, the devices utilize either a Si_xN_y or Al_2O_3 based stress-compensating frame discussed in sections 3 and 4 that is used to tune the stress of the detector membrane. The details of each layer are included in Figure 7. The metal-poly-Si absorber stack is patterned into a grid with plasma dry etching to control the optical impedance of the grid and to allow for easier removal of the underlying sacrificial oxide during device fabrication. For all device types the detector is electrically isolated from the substrate by suspension over an optical cavity, which acts as an optical resonator. The optical cavity and absorber form a quarter-wave resistive absorber (see section 2.2). The detector's performance can be optimized for specific wavelengths by varying the depth of the cavity. Here the detector output was maximized for the target LWIR wavelength of 10 μm by setting the cavity depth to 2.5 μm .

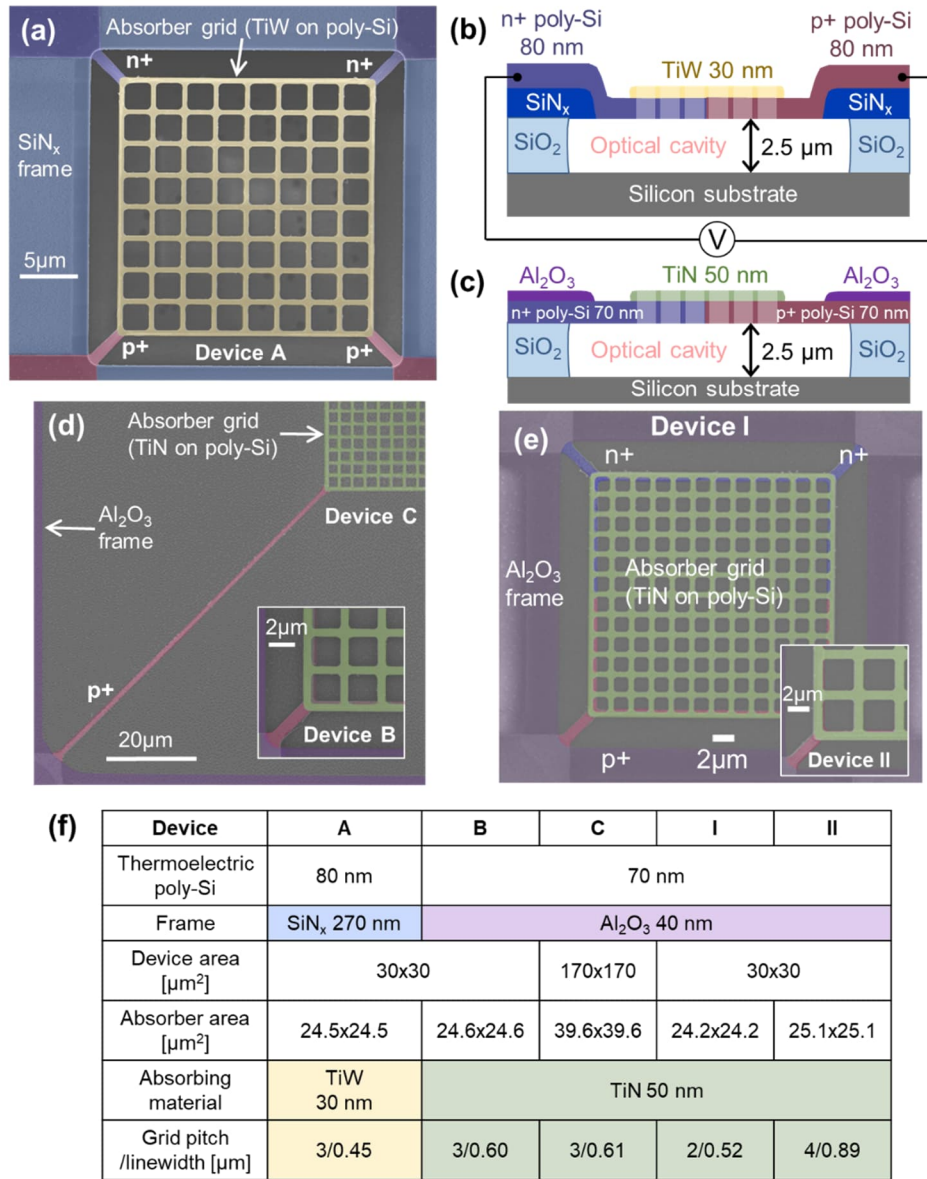


Figure 7. Pseudo-colored scanning-electron micrographs (a, d, e) and cross-sectional schematics (b, c) of nano-thermoelectric infrared bolometers A-C⁴ and I-II⁷. The dimensions and material characteristics of the device layers are included in Table (f).

The nano-thermoelectric bolometers have been fabricated on 150 mm single-side polished p-type (1 – 50 Ωm) silicon wafers^{4,7}. All wafers started with the deposition of 2.5µm sacrificial SiO₂ using LPCVD with tetraethyl orthosilicate (TEOS). In the case of the wafers with SiN_x stress-compensating frame, the SiN_x was deposited using LPCVD and patterned using plasma dry etching. After SiN_x deposition, the poly-Si layer was deposited by LPCVD, followed by patterned implantation and poly-Si plasma dry etching. In the case of the Al₂O₃ devices, the poly-Si was deposited and processed first, followed by atomic layer deposition of Al₂O₃, which was patterned using wet etching. For the SiN_x and Al₂O₃ detectors the absorber metals were sputtered: 30 nm TiW and 50 nm TiN, respectively. The absorber metal was patterned using plasma dry etching to form the detector grid and to enable access to selectively remove the underlying sacrificial oxide to suspend the detector membrane. Finally, the sacrificial SiO₂ is etched using HF-vapor to release the devices and to form the optical cavity.

The opto-electro-thermal characteristics of the fabricated nano-thermoelectric infrared bolometers are summarized in Table 3. The differences in the device speeds are determined by the absorber sizes (A_{abs}) and beam dimensions as they determine the thermal masses and thermal conductances. The small devices (A, B, I-II) are remarkably fast (for thermal detectors) with thermal time constants τ of 66 μs (Dev. A) and around 200 μs (larger devices) and the corresponding thermal cutoff frequencies around 2400 Hz and 800 Hz, respectively. These detectors allow infrared signals up to several kHz to be measured, depending on the required signal-to-noise ratios.

Table 3. Opto-electro-thermal characteristics of the nano-thermoelectric infrared bolometers^{4,7}.

Device	A	B	C	I	II
Thickness of thermoelectric poly-Si	80 nm	70 nm			
Absorbing material	TiW 30 nm	TiN 50 nm			
Absorber area [μm^2]	24.5×24.5	24.6×24.6	39.6×39.6	24.2×24.2	25.1×25.1
Measured thermal time constant τ [μs]	66	190	3596	197	208
Total bolometer resistance R_{tot} [$\text{k}\Omega$]	50.0	11.9	86.4	6.5	9.1
Resistance of thermoelectric beams R_{beams} [$\text{k}\Omega$]	2.5	2.7	58.1	2.7	2.7
Measured responsivity R_V to 200 °C BB radiation [V/W]	179	494	2930	334	398
Optical noise equivalent power ^b (NEP) [$\text{pW}/\text{Hz}^{1/2}$]	160	28	13	31	31
Optical NEP determined by R_{beams} only ^{b,c} [$\text{pW}/\text{Hz}^{1/2}$]	36	13	11	20	17
Specific detectivity ^{b,c} D^* [$10^7 \text{ cmHz}^{1/2}/\text{W}$]	1.5	8.7	30.9	7.9	8.2
D^* determined by R_{beams} only ^{b,d} [$10^7 \text{ cmHz}^{1/2}/\text{W}$]	6.9	18.4	37.7	12.3	15.1

^b200 °C blackbody (BB) radiation.

^cSensitivity determined by total resistance, which is limited by additional series resistance such as contact resistance. Calculated using eq. (3) with $R = R_{\text{tot}}$.

^dLimiting sensitivity determined by the resistance of the thermoelectric beams. Calculated using eq. (3) with $R = R_{\text{beams}}$.

The differences in the responsivities are caused by the slight differences in the total Seebeck coefficient S of the nanomembrane and larger differences in the absorber areas A_{abs} , thermal conductivities G_{th} , and absorber efficiencies η , which are, in turn, caused by differences in the non-optimal matching to vacuum impedance^{4,7} (see section 2.2). The absorber efficiency can be improved by optimizing the absorber grid dimensions for better impedance matching and by improving the reflectance of the back reflector⁴. The fact that relatively high responsivities were obtained demonstrates how well the quarter-wave absorber can work even with non-optimal parameters.

The voltage noise of these bolometers is due to the Johnson-Nyquist noise⁴, which is determined by the total resistance of the bolometer R_{tot} [see eq. (3)]. As Table 3 shows, the optical NEPs of the devices are determined by their responsivities R_V and the total resistances R_{tot} . Notably, the optical NEP of Device C is the same as the electrical NEP of electro-thermal device SC-B (Table 2).

The total resistance R_{tot} comprises of the resistance of the thermoelectric beams R_{beams} , the resistance of the absorber grid, and the potential contact resistance between the absorber metal and the poly-Si. The resistance of the absorber grid has ideally only little contribution to the total resistance of the devices as the effective sheet resistance of the absorber grid is close to the vacuum impedance (377Ω)⁴. The poly-Si–metal contact resistance can be high, as in the case of Device A

(see Table 3). Therefore, the optimization of contact resistance by material and process development is crucial. The performance can be further improved by geometrical optimization of the thermoelectric beams for improved \bar{ZT}^4 . Optimization of the bolometer resistance and optical absorption will improve the optical NEPs of these bolometers to the same and lower level as the electrical NEPs of the electro-thermal devices.

To compare the nano-thermoelectric infrared bolometers with the state-of-the-art thermal detector technologies, the time constant and specific detectivities D^* of commercial and non-commercial LWIR bolometers are plotted in Figure 8. Our bolometers are fast, and the fastest detector in the graph is Device A. Our devices are also relatively sensitive, and by optimization of the device resistance and optical absorption their specific detectivities can be further improved⁴. In addition, we estimate that by utilizing 9-nm-thick poly-Si nanomembranes, we could, depending on the device design, realize either faster or more sensitive detectors than the state of the art.

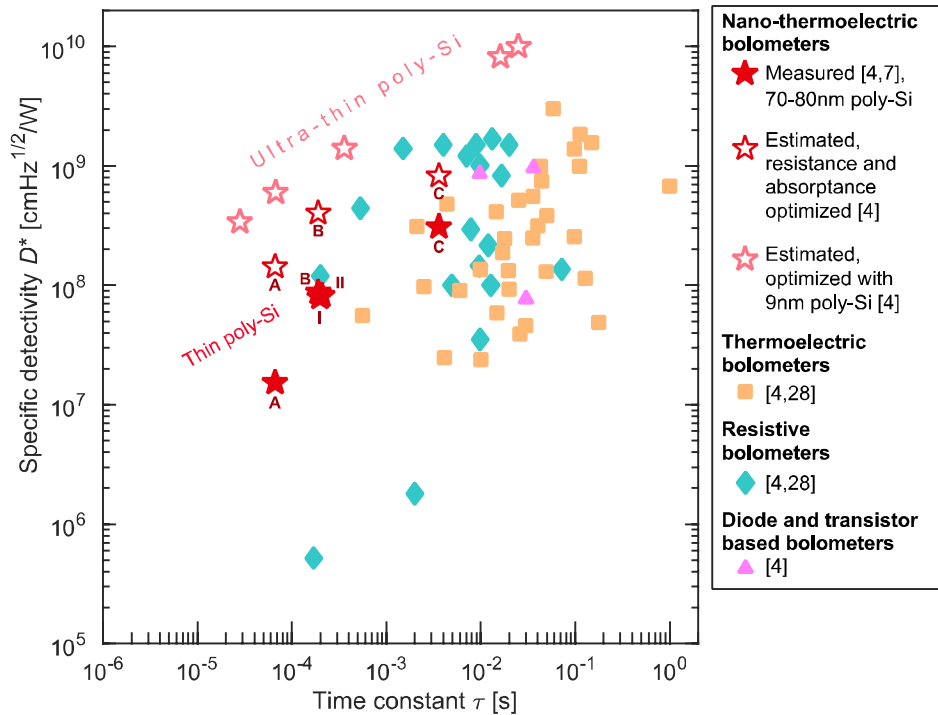


Figure 8. Time constants τ and specific detectivities D^* of the nano-thermoelectric bolometers^{4,7} and of commercial and non-commercial LWIR bolometers^{4,28}.

6. ESTIMATION OF PERFORMANCE OF NANO-THERMOELECTRIC BOLOMETERS

We have used the device models of section 2.1 to show that silicon and metal nanomembranes can be used as high-performance active materials of thermoelectric bolometers^{29,30}. The effect of the membrane thickness on the device performance is shown in Fig. 9, where D^* and τ of detectors with Ti absorbers and 3 different absorber sizes and leg geometries are plotted. The absorber area A_{abs} and the leg geometries defined by the number of squares in the legs N , determine the speed of the detectors via the thermal mass (C_{th}) and the thermal link (G_{th}). A_{abs} also determines D^* as it governs the amount of radiation absorbed. The membrane thickness t_{TE} has a profound effect on the device performance as it determines the thermal mass and the thermal conductivity of the nanomembrane (see Fig. 5). When t_{TE} decreases, G_{th} decreases both due to the geometric effect ($G_{\text{th}} \propto t_{\text{TE}}$) and the drastic decrease of thermal conductivity of the nanomembrane, which leads to increase in \bar{ZT} . These leads to increase in D^* with decreasing t_{TE} . The dependence of $\tau = C_{\text{th}}/G_{\text{th}}$ [eq. (1)] is more complex as both G_{th} and C_{th} decrease with decreasing t_{TE} . Dependencies of further device parameters are discussed in Refs. [29, 30]. In overall, these calculations show that in infrared detectors, nano-

thermoelectric silicon has the potential to realize the detector performance close to the fundamental limit determined by the thermal fluctuation noise only⁴².

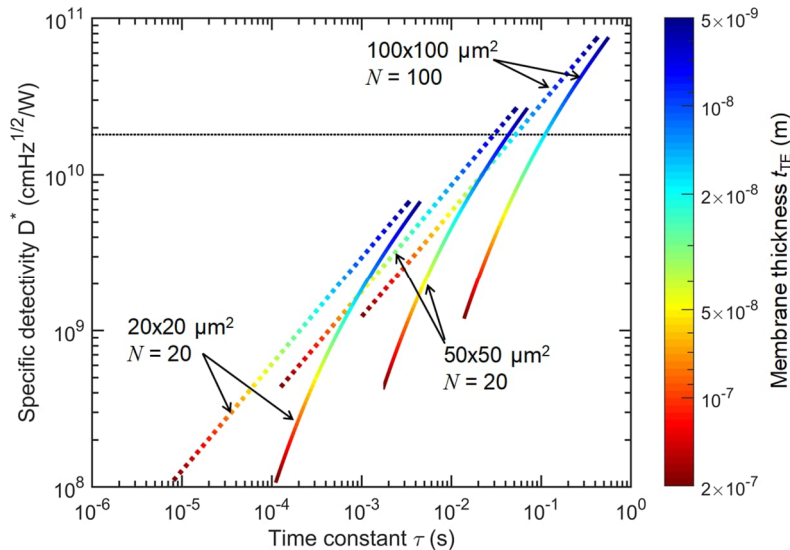


Figure 9. Calculated specific detectivities D^* and thermal time constants τ of Si-nanomembrane-based thermoelectric bolometers with 10 nm Ti absorber and different absorber areas and leg geometries as functions of the membrane thickness t_{TE} ²⁹. The absorber area A_{abs} and the number of squares in the n- and p-type thermoelectric legs N are indicated in the graph. The dotted lines are the case where the absorber comprises of Ti only, and the solid lines are the case where the absorber is made of both Ti and Si nanomembranes. Resistivity of 1 m Ω cm and the thermal conductivity model of Fig. 5 was used for the Si-nanomembrane in the calculations. The black dashed line is the background radiation limit for thermal detectors in the full spectrum and half space case at 300 K⁴². Beyond this limit the estimated detector D^* is limited only by the external background noise. Further parameter values and details are given in Ref. [29].

7. CONCLUSIONS

Phonon-engineered silicon nanomembranes enable the realization of cost-effective and high-performance electro-thermal devices for thermal experiments and infrared bolometers for a wide range of optical imaging and sensing applications such as night vision and optical chemical sensing. The nano-thermoelectric IR bolometer design is based on the quarter-wave resistive absorber, where the wavelength range of interest can be selected by the cavity depth and absorber design. In principle, designs could be made for the entire infrared range. We have shown that the nano-thermoelectric infrared bolometer technology can exceed the state-of-the-art thermal detectors.

ACKNOWLEDGEMENTS

This work has been financially supported by Business Finland co-innovation project RaPtor (No. 6030/31/2018), European Union Future and Emerging Technologies (FET) Open under Horizon 2020 program (Grant Agreement No. 766853, project EFINED), and the Academy of Finland (Grant No. 342586). The work of Jonna Tiira was supported by Academy of Finland (Grant No. 324838). We acknowledge gratefully the technical assistance of Teija Häkkinen in device fabrication.

REFERENCES

- [1] Budzier, H. and Gerlach, G., [Thermal infrared sensors: theory, optimisation and practice], Wiley (2011).
- [2] Baldini, F., Chester, A. N., Homola, J. and Martellucci S., [Optical Chemical Sensors], Springer (2006).
- [3] Popa, D. and Udrea, F., "Towards Integrated Mid-Infrared Gas Sensors," *Sensors* 19, 2076 (2019).
- [4] Varpula, A., Tappura, K., Tiira, J., Grigoros, K., Kilpi, O.-P., Sovanto, K., Ahopelto, J. and Prunnila, M., "Nano-thermoelectric infrared bolometers," *APL Photonics* 6, 036111 (2021).
- [5] Varpula, A., Timofeev, A. V., Schepetov, A., Grigoros, K., Hassel, J., Ahopelto, J., Ylilammi, M. and Prunnila M., "Thermoelectric thermal detectors based on ultra-thin heavily doped single-crystal silicon membranes," *Appl. Phys. Lett.* 110, 262101 (2017).
- [6] Varpula, A., Grigoros, K., Tappura, K., Timofeev, A.V., Shchepetov, A., Hassel, J., Ahopelto, J. and Prunnila, M., "Silicon Based Nano-Thermoelectric Bolometers for Infrared Detection," *Proc. Euroensors*, 2(13), 894 (2018).
- [7] Varpula, A., Murros, A., Sovanto, K., Rantala, A., Gomes Martins, D., Tappura, K., Tiira, J., and Prunnila, M., "Uncooled nano-thermoelectric bolometers for infrared imaging and sensing," *Proc. SPIE 12417, Optical Components and Materials XX*, 124170U, 124170U (2023).
- [8] Chávez-Ángel, E., Reparaz, J. S., Gomis-Bresco, J., Wagner, M. R., Cuffe, J., Graczykowski, B., Shchepetov, A., Jiang, H., Prunnila, M., Ahopelto, J., Alzina, F. and Sotomayor-Torres, C. M., "Reduction of the thermal conductivity in free-standing silicon nano-membranes investigated by non-invasive Raman thermometry," *APL Mater.* 2, 012113 (2014).
- [9] Mangold, C., Neogi, S. and Donadio, D., "Optimal thickness of silicon membranes to achieve maximum thermoelectric efficiency: A first principles study," *Appl. Phys. Lett.* 109 (5), 053902 (2016).
- [10] Asheghi, M., Leung, Y. K., Wong, S. S. and Goodson, K. E., "Phonon-boundary scattering in thin silicon layers," *Appl. Phys. Lett.* 71 (13), 1798-1800 (1997).
- [11] Ju, Y. S. and Goodson, K. E., "Phonon scattering in silicon films with thickness of order 100 nm," *Appl. Phys. Lett.* 74 (20), 3005-3007 (1999).
- [12] Liu, W., Asheghi, M., "Thermal conduction in ultrathin pure and doped single-crystal silicon layers at high temperatures," *Journal of Applied Physics* 98 (12), 123523 (2005).
- [13] Liu, X., Wu, X., Ren, T., "In situ and noncontact measurement of silicon membrane thermal conductivity," *Appl. Phys. Lett.* 98 (17), 174104 (2011).
- [14] Balandin, A. and Wang, K., "Significant decrease of the lattice thermal conductivity due to phonon confinement in a free-standing semiconductor quantum well," *Phys. Rev. B* 58, 1544-1549 (1998).
- [15] Huang, M.-J., Chang, T.-M., Chong, W.-Y., Liu, C.-K. and Yu, C.-K., "A new lattice thermal conductivity model of a thin-film semiconductor," *International Journal of Heat and Mass Transfer* 50 (1-2), 67-74 (2007).
- [16] Lü, X., "Lattice thermal conductivity of Si nanowires: Effect of modified phonon density of states," *Journal of Applied Physics* 104 (5), 054314 (2008).
- [17] Tang, G. H., Zhao, Y., Zhai, G. X. and Bi, C., "Phonon boundary scattering effect on thermal conductivity of thin films," *Journal of Applied Physics* 110 (4), 046102 (2011).
- [18] Liu, W. and Asheghi, M., "Phonon-boundary scattering in ultrathin single-crystal silicon layers," *Appl. Phys. Lett.* 84 (19), 3819-3821 (2004).
- [19] Martin, P., Aksamija, Z., Pop, E. and Ravaioli, U., "Impact of Phonon-Surface Roughness Scaling on Thermal Conductivity of Thin Si Nanowires," *Phys. Rev. Lett.* 102, 125503 (2009).
- [20] Yu, J.-K., Mitrovic, S., Tham, D., Varghese, J. and Heath, J. R., "Reduction of thermal conductivity in phononic nanomesh structures," *Nature Nanotech* 5, 718-721 (2010).
- [21] Tang, J., Wang, H.-T., Lee, D. H., Fardy, M., Huo, Z., Russell, T. P. and Yang, P., "Holey Silicon as an Efficient Thermoelectric Material," *Nano Letters* 10 (10), 4279-4283 (2010).
- [22] Hicks, L. D. and Dresselhaus, M. S., "Effect of quantum-well structures on the thermoelectric figure of merit," *Phys. Rev. B* 47, 12727 (1993).
- [23] Vo. T. T. M., Williamson, A. J., Lordi, V. and Galli, G., "Atomistic Design of Thermoelectric Properties of Silicon Nanowires," *Nano Letters* 8 (4), 1111-1114 (2008).
- [24] Ikeda, H. and Salleh, F., "Influence of heavy doping on Seebeck coefficient in silicon-on-insulator," *Appl. Phys. Lett.* 96 (1), 012106 (2010).

- [25] Neophytou, N., Zianni, X., Kosina, H., Frabboni, S., Lorenzi, B. and Narducci, D., "Simultaneous increase in electrical conductivity and Seebeck coefficient in highly boron-doped nanocrystalline Si," *Nanotechnology* 24, 205402 (2013)
- [26] Neophytou, N., Karamitaheri, H. and Kosina, H., "Atomistic calculations of the electronic, thermal, and thermoelectric properties of ultra-thin Si layers," *J Comput Electron* 12, 611–622 (2013).
- [27] Richards, P. L., "Bolometers for infrared and millimeter waves," *J. Appl. Phys.* 76, 1 (1994).
- [28] Dillner, U., Kessler, E. and Meyer, H.-G., "Figures of merit of thermoelectric and bolometric thermal radiation sensors," *J. Sens. Sens. Syst.* 2, 85 (2013).
- [29] Varpula, A., Tappura, K., Tiira, J., Grigoras, K., Viherkanto, K., Ahopelto, J. and Prunnila, M., "High-performance infrared thermoelectric bolometers based on nanomembranes," *Proc. SPIE* 11289, Photonic and Phononic Properties of Engineered Nanostructures X, 112891O (2020).
- [30] Varpula, A., Timofeev, A. V., Schepetov, A., Grigoras, K., Ahopelto, J. and Prunnila M., "Thermoelectric bolometers based on silicon membranes," *Proc. SPIE* 10246, Smart Sensors, Actuators, and MEMS VIII, 102460L (2017).
- [31] Salisbury, W. W., "Absorbent body for electromagnetic waves," U. S. Patent 2,599,944 (1952).
- [32] Talghader, J. J., Gawarikar, A. S. and Shea, R. P., "Spectral selectivity in infrared thermal detection," *Light Sci. Appl.* 1, e24 (2012).
- [33] Fante, R. L. and McCormack, M. T., "Reflection properties of the Salisbury screen," *IEEE Trans. Antennas Propagat.* 36(10), 1443–1454 (1988).
- [34] Katsidis, C. C. and Siapkias, D. I., "General transfer-matrix method for optical multilayer systems with coherent, partially coherent, and incoherent interference," *Appl. Opt.*, AO 41(19), 3978–3987 (2002).
- [35] Born, M. and Wolf, E., [Principles of Optics: Electromagnetic Theory of Propagation, Interference and Diffraction of Light], Elsevier (2013).
- [36] Glassbrenner, C. J. and Slack, G. A., "Thermal Conductivity of Silicon and Germanium from 3°K to the Melting Point," *Phys. Rev.* 134, A1058–A1069 (1964).
- [37] Neogi, S., Reparaz, J. S., Pereira, L. F. C., Graczykowski, B., Wagner, M. R., Sledzinska, M., Shchepetov, A., Prunnila, M., Ahopelto, J., Sotomayor-Torres, C. M., and Donadio, D., "Tuning Thermal Transport in Ultrathin Silicon Membranes by Surface Nanoscale Engineering," *ACS Nano* 9 (4), 3820 (2015).
- [38] Boukai, A., Bunimovich, Y., Tahir-Kheli, J., Yu, J.-K., Goddard III, W. A. and Heath, J. R., "Silicon nanowires as efficient thermoelectric materials," *Nature* 451, 168–171 (2008).
- [39] Shchepetov, A., Prunnila, M., Alzina, F., Schneider, L., Cuffe, J., Jiang, H., Kauppinen, E. I., Sotomayor Torres, C. M. and Ahopelto, J., "Ultra-thin free-standing single crystalline silicon membranes with strain control," *Appl. Phys. Lett.* 102, 192108 (2013).
- [40] Varpula, A., Renahy, D., Grigoras, K., Tappura, K., Timofeev, A. V., Shchepetov, A., Hassel, J., Ahopelto, J., Gomés, S., and Prunnila, M., "Silicon nano-thermoelectric detectors for sensing and instrumentation applications," *Nanoscale and Microscale Heat Transfer VI (NMHT-VI)*, Eurotherm seminar No 111, Levi, Lapland, Finland, 2 – 7 December 2018.
- [41] Gomès, S., Assy, A., Chapuis, P.-O., "Scanning thermal microscopy: A review," *Phys. Status Solidi* 212 (3), 477 (2015).